

The Dynamics of Boundary Layer Jets within the Tropical Cyclone Core. Part I: Linear Theory

JEFF KEPERT

Bureau of Meteorology Research Centre, Melbourne, Victoria, Australia

(Manuscript received 27 July 1998, in final form 16 November 2000)

ABSTRACT

Observations of wind profiles within the tropical cyclone boundary layer have until recently been quite rare. The recent massive increase in observations due to the operational implementation of the global positioning system dropwindsonde has emphasized that a low-level wind speed maximum is a common feature of the tropical cyclone boundary layer. Here is proposed a mechanism for producing such a maximum, whereby strong inward advection of angular momentum generates the supergradient flow. The processes that maintain the necessary inflow against the outward acceleration resulting from gradient wind imbalance are identified as being (i) vertical diffusion, (ii) vertical advection, and (iii) horizontal advection. Two complementary tools are used to diagnose the properties and dynamics of the jet. The first, presented here, is a linear analytical model of the boundary layer flow in a translating tropical cyclone. It is an extension of the classical Ekman boundary layer model, as well as of earlier work on stationary vortex boundary layers. This simplifies the vertical diffusion, omits the vertical advection, and linearizes the horizontal advection. The solution is shown to have three components, a symmetric one due to the cyclone, and two asymmetric ones that result from the interaction of the moving cyclone with the earth's surface. The asymmetric components are shown to be equivalent to a frictionally stalled inertia wave. It is argued that an Ekman-type model may be appropriate in tropical cyclones since diurnal effects are weak or absent, turbulence is dominantly shear-generated, and baroclinicity is weak.

The jet is similar to the supergeostrophic flow found at the top of the classical Ekman spiral. It is only a few percent supergradient in the linear model, although it is shown that the neglect of vertical advection substantially reduces the strength. The jet height scales as $(2K/I)^{1/2}$, where K is the turbulent diffusivity and I the inertial stability, modulated by a function of a dimensionless parameter. It is typically several hundreds of meters in the cyclone core, and increases with radius. In a moving storm, the jet is most supergradient—several times stronger than in a stationary storm—at the eyewall to the left and front of the storm (in the Northern Hemisphere), as well as extending into a significant area around to the left of the storm. It is, however, much less marked to the right, where the strongest near-surface winds are found.

The factor for reducing upper winds to a near-surface equivalent, which is frequently used in operational work, is shown to have a substantial spatial variability. Larger values are found near the eye, due to the symmetric component of the solution. There is also a marked overall increase from right to left of the storm in the Northern Hemisphere.

The second tool used to diagnose the jet, to be presented in Part II of this paper, is a high-resolution, dry, hydrostatic, numerical model using the full set of primitive equations. It therefore includes those terms omitted in the linear model, and will be seen to produce a markedly stronger jet, more consistent with the observations.

1. Introduction

The simple view of mass-wind balance in a tropical cyclone—that gradient balance applies everywhere except in the boundary layer—appears to be well supported by observations (La Seur and Hawkins 1963; Hawkins and Rubsam 1968; Willoughby 1990, 1991). While there are some dissenting voices (Gray 1967, 1991) the differences seem to be an artifact of the analysis process. The correspondingly simple view of the boundary layer would be of a steady decrease in wind

speed from gradient flow at the top, toward something variously estimated at 0.7 to 0.9 times that, at 10 m (Powell 1980; Powell 1982; Powell 1987; Powell et al. 1991; Powell et al. 1996), together with a progressive turning of the wind direction toward the storm centre. Although the use of a wind reduction factor is well supported by the data—albeit with significant variation in the value of the constant in different studies—there is some evidence to contradict the idea of a monotonic profile. Until very recently, the number of observations of wind profiles in the tropical cyclone boundary layer was not large, due to the difficulty of taking measurements there. However, a considerable proportion of those early observations show the presence of low-level jets, variously reported as being at 60 m (Wilson 1979),

Corresponding author address: Dr. Jeff D. Kepert, Bureau of Meteorology Research Centre, GPO Box 1289K, Melbourne, Vic 3001, Australia.
E-mail: j.kepert@bom.gov.au

200 m (Korolev et al. 1990), and 550 m (Moss and Merceret 1976). In the recent past, the advent of the GPS dropsonde (Hock and Franklin 1999) has yielded a wealth of new data on this phenomenon. For instance, Black and Shay (1998) in an initial report on recent observations from this instrument, state that “nearly all high wind soundings show this feature [a low-level jet].” Finally, the high-resolution modeling study of Li et al. (1997) shows a similar feature.

Such features are potentially of considerable practical importance. If the additional momentum was advected toward the surface by, say, a convective downdraft, it could have a considerable impact on surface damage. It is also important to operational forecasts and warnings, and should probably be considered in the design of high-rise structures. In areas where aircraft reconnaissance is available, it is necessary to estimate a near-surface wind from flight level data, and various models have been used to “reduce” the flight level winds to the surface (Powell 1980). Without exception, these models assume a monotonic profile. A similar application often occurs in storm surge modeling, where a suitable parametric gradient wind field and profile model are used to determine a surface wind field to force the ocean model (e.g., Hubbert et al. 1991). Clearly, departures from monotonicity will impact the accuracy of these reductions. In this context it is interesting to note that the profile models do not perform all that well. In fact, when Powell (1980) tested a number of them against aircraft and buoy data, he found that simply multiplying the flight level wind by 0.8 was as good or better predictor of the near-surface wind speed than any of the physically based models.

The lack of success of profile models is perhaps not surprising. Extrapolation of parameterizations derived for more benign conditions to the extreme winds of a tropical cyclone may not be valid. With lowest flight levels in the vicinity of 500 m, the assumptions of surface layer similarity theory are almost certainly violated. In fact, as we will see, 500 m is toward the top of the boundary layer in the tropical cyclone core. Moreover, the necessary assumption for any one-dimensional model of horizontal homogeneity is unlikely to be met in the strong gradients near the cyclone core, and at landfall. This problem is exacerbated since the adjustment time for the profile to attain equilibrium due to changes in surface conditions or gradient level wind will be longer for a deeper profile. On the other hand, the large momentum fluxes at these wind speeds is a factor in favor of relatively rapid adjustment.

Explanations of the cause of these low level wind maxima have been sought by analogy with the well-known nocturnal jet (Blackadar 1957). Here, nocturnal cooling produces such a strong stabilisation of the lower boundary layer that the flow above is effectively decoupled from the surface. The frictionally induced ageostrophic part of the flow then undergoes an inertial oscillation, until it is aligned with, and adds to, the

geostrophic part of the flow, typically producing the strongest wind shortly before sunrise and at a height of a few hundred meters. Black and Holland (1995) claimed to have observed this process in an Australian tropical cyclone. Recent observations of air–sea temperature difference in cyclone cores, where the air is cooled to several degrees below the sea surface temperature (Korolev et al. 1990; Black et al. 1993; Cione et al. 2000), have furthered this speculation. Clearly the analogy is not exact—the surface wind does not go to zero, and anemometer traces provide plentiful evidence of strong turbulence at the surface—so decoupling cannot be complete. Moreover, the greater shear and lesser cooling in the cyclone leave the Richardson number much closer to zero than in the nocturnal boundary layer, with therefore a much larger vertical momentum transport. This analysis will be extended in Kepert and Wang (2001, henceforth called Part II).

The possibility of supergradient winds in the boundary layer has received its most thorough treatment to date in Shapiro (1983), who used a slab model to calculate the depth-averaged boundary layer wind field for stationary and moving storms, and found a small area of boundary layer supergradient flow just inside the gradient level radius of maximum winds in a stationary storm, and located toward the front and left of a moving storm. Willoughby (1991) presented a relatively crude calculation with an assumed cross-contour flow angle in the boundary layer, which also supported the possibility, while Mitsuta et al. (1988) presented observations of a supergradient near-surface wind in Typhoon Vera of 1977. In each case, the winds were approximately 10% supergradient. Finally, Rosenthal (1962) and Eliassen and Lystad (1977) presented Ekman-like models for the boundary layer of a stationary vortex. Their linear models produced only weakly supergradient flow in the upper part of the boundary layer. Our analysis extends theirs in several important areas, including the effects of motion, the role of nonlinearities in producing a jet of realistic strength, and the application to a wider and more realistic range of tropical cyclonelike vortices.

Here we discuss a physical mechanism for supergradient flow in the tropical cyclone boundary layer. While this mechanism does not depend on changes in the static stability profile, we do not discount a possible secondary role for these at this time. Rather, our purpose is to present a simpler explanation for these features, and argue therefore that our models contain the essential physics. In section 2, we begin with a physical discussion of some of the necessary conditions for a jet in an axisymmetric storm and then develop a linear analytic model of the boundary layer of a moving tropical cyclone. Section 3 applies the linear theory to stationary tropical cyclones, while section 4 explores the effects of cyclone motion. Conclusions and further discussion are in section 5. Part II of this paper introduces our second tool, a high-resolution model of the tropical cyclone boundary layer. This is used to study nonlinear

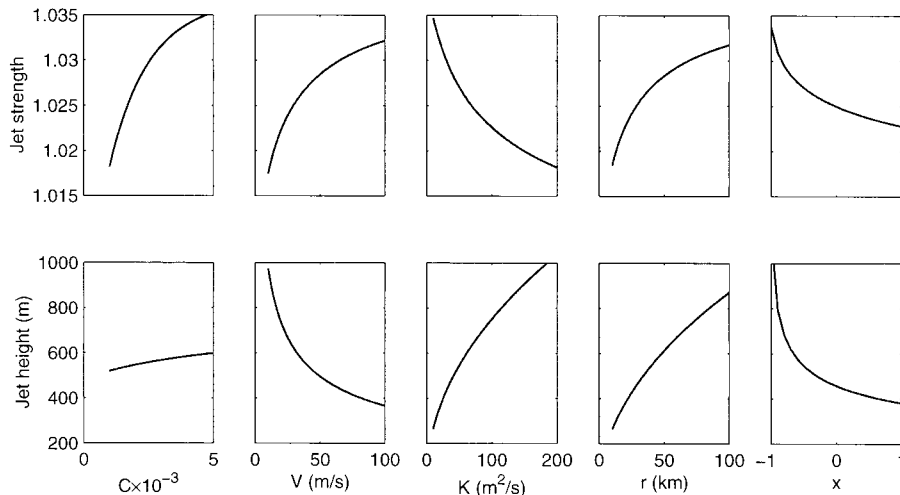


FIG. 1. The variation of relative jet strength (top) and jet height (bottom) with various parameters in the linear model, according to (27). For each pair of graphs, the parameters not varying have values $C = 0.002$, $V = 40 \text{ m s}^{-1}$, $K = 50 \text{ m}^2 \text{ s}^{-1}$, $r = 40 \text{ km}$, and $x = -0.5$.

effects in detail, as well as apply a more realistic representation of the turbulence.

2. Discussion and linear model

a. Motivation

The budget equation for absolute angular momentum about the storm center, M_a , defined by

$$M_a = rv + \frac{1}{2}fr^2, \quad (1)$$

is

$$\frac{DM_a}{Dt} = -\frac{\partial\phi}{\partial\lambda} + K\left[\nabla^2 M_a + \frac{2}{r}\left(\frac{\partial u}{\partial\lambda} - \frac{\partial M_a}{\partial r}\right)\right], \quad (2)$$

so M_a changes only through horizontal advection, azimuthal pressure gradients, and frictional torques. Here, u and v are the radial and azimuthal wind components respectively in the storm-centered cylindrical coordinate system (r, λ, z) , ϕ is the geopotential, f the Coriolis parameter, $\nabla^2 = \partial^2/\partial r^2 + 1/r\partial/\partial r + 1/r^2\partial^2/\partial\lambda^2 + \partial^2/\partial z^2$ the Laplacian operator in cylindrical coordinates, K the turbulent diffusivity for momentum (assumed constant), and $D/Dt = \partial/\partial t + u\partial/\partial r + v\partial/\partial\lambda + w\partial/\partial z$ is the rate of change following the parcel. The use of M_a is convenient for physical interpretation, since the Coriolis and centripetal terms in the azimuthal velocity equation are absorbed in the definition of M_a .

For a steady-state, symmetric, stationary storm in a quiescent environment, we thus have a balance at all levels between radial advection, vertical advection, and turbulent diffusion of M_a . In an inertially neutral storm, the radial gradient of angular momentum (and hence its radial advection) is zero, while M_a increases outward in an inertially stable storm. We may thus expect that a

sufficiently strong combination of inertial stability and inflow could produce a steady supergradient flow in such a storm.

However, the balance for the radial flow must also be considered. If the azimuthal component is supergradient, the imbalance between pressure, Coriolis and centripetal terms will tend to produce an outward acceleration of the radial wind at that level. Such a reduction or reversal of the inflow would upset the balance in the previous paragraph and lead to a weakening of the jet. Examining the balance equation for the radial flow in such a storm,

$$\begin{aligned} u\frac{\partial u}{\partial r} + w\frac{\partial u}{\partial z} - \left(f + \frac{v}{r}\right)v \\ = -\frac{\partial\phi}{\partial r} + K\left[\nabla^2 u - \frac{1}{r^2}\left(u + 2\frac{\partial v}{\partial\lambda}\right)\right], \quad (3) \end{aligned}$$

we see the possible candidates for maintenance of the inflow against the imbalance in the gradient wind part of the equation are inward and vertical advection, and turbulent diffusion. One possibility is that the inflow increases outward from the storm centre, and is thus being maintained by self-advection. Another is that the inflow is greater below the level of the jet (above is implausible), and is being maintained at the level of the jet by upward diffusion, and perhaps also upward advection if the jet is located in an updraft. We expect the contribution of turbulent horizontal diffusion to be small.

We now incorporate the ideas from this physical reasoning into a linear analytic model of the tropical cyclone boundary layer. In it (and the numerical model to follow in Part II), we regard the boundary layer as the frictional response to a known, steady-state, tropical cy-

clone wind field in the “free atmosphere.” We specifically choose to ignore the influence that changes in the boundary layer structure may have on the cyclone as a whole. While these clearly exist—for example, the pattern of boundary layer convergence will affect the distribution of convection and hence heating—the scope of this study is rather to explore just one side of what is undoubtedly a two-way interaction. We opt also not to attempt to resolve the effects of convection on the boundary layer, concentrating rather on larger scales. While studies (e.g., Powell 1990a,b; Barnes and Powell 1995) have shown significant modulation of boundary layer structure in the vicinity of rainbands, on scales comparable to the width of the band, we prefer to focus at present on building an understanding of the larger-scale features of the tropical cyclone boundary layer.

Consistent with our focus on the boundary layer as a response to the “free atmosphere” flow, our representation of that by a parametric pressure field, and our neglect of convection, we exclude moisture from the model. Had it been included, its sole role (apart from that of passive tracer) would be a tiny contribution to the height variation of pressure, through the hydrostatic equation.

Finally, we ignore also transient features that may arise due to instabilities in the prescribed vortex flow. Again, while these may well be important in the real atmosphere, we are here concerned with determining the steady, frictionally forced flow beneath an idealized tropical cyclone.

b. A linear model of the tropical cyclone boundary layer

Here we develop a linear analytical model for the boundary layer flow in a tropical cyclone. The formulation and solutions have some features in common with the well-known Ekman spiral model of the boundary layer, although with some important differences. The symmetric part, applicable to a stationary vortex, is similar to the model proposed by Eliassen and Lystad (1977), although they obtained numerical rather than analytical solutions. Also, the most intense vortex they considered, with a Rossby number of 20, is below tropical cyclone strength. However, their model has been verified in more intense cyclones by Snell and Montgomery (1999). The symmetric component was also considered by Rosenthal (1962), although with a less accurate linearization of the surface boundary condition. We will study the sensitivity of the solution to a wider range of conditions than these earlier investigators. A significant advance here is the introduction of the asymmetric components, relevant to a moving storm, which do not appear to have been investigated before.

The horizontal momentum equations for a steady-state vortex with constant vertical turbulent diffusivity and no horizontal diffusion, in cylindrical coordinates moving with the vortex, are

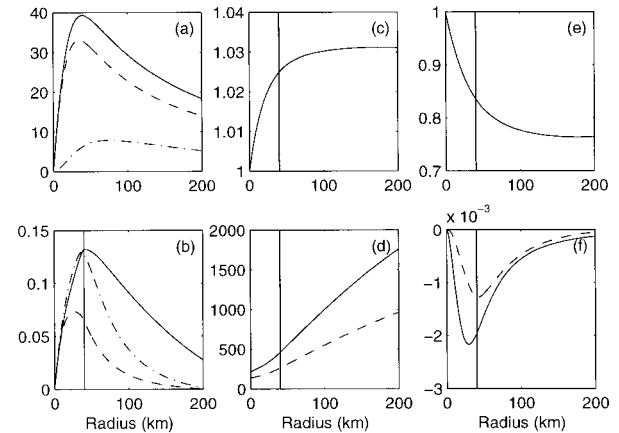


FIG. 2. Radial profiles of (a) gradient wind (solid), surface azimuthal (dashed), and inflow (dash-dotted) components; (b) vertical velocity at 200 m (dashed), 500 m (dash-dot), and infinity (solid); (c) jet strength relative to the gradient wind; (d) jet height (solid) and depth scale δ_0 (dashed); (e) surface wind reduction factor; and (f) forcing of inflow at the jet height by vertical diffusion (solid) and vertical advection (dashed). The cyclone is prescribed by the analytic model of Holland (1980) with $r_{\max} = 40$ km, $V_{\max} = 40$ m s^{-1} , and $b = 1.3$, with the eye modification described in the text. Other parameters are $C = 0.002$, $K = 50$ m² s^{-1} , latitude 15°N.

$$u \frac{\partial u}{\partial r} + \frac{v}{r} \frac{\partial u}{\partial \lambda} + w \frac{\partial u}{\partial z} - \left(f + \frac{v}{r} \right) v = - \frac{\partial \phi}{\partial r} + K \frac{\partial^2 u}{\partial z^2}$$

$$u \frac{\partial v}{\partial r} + \frac{v}{r} \frac{\partial v}{\partial \lambda} + w \frac{\partial v}{\partial z} + \left(f + \frac{v}{r} \right) u = K \frac{\partial^2 v}{\partial z^2}. \quad (4)$$

We denote the symmetric gradient level flow by V , which is assumed to be in balance with the pressure gradient, $fV + V^2/r = \partial\phi/\partial r$. Additionally, we have assumed that the vortex is moving with the environmental flow U_e , which is in geostrophic balance. When subtracting off the vortex motion to obtain (4), we also subtract off the corresponding environmental pressure gradient, and so there is thus no $\partial\phi/\partial\lambda$ term. Replacing v by $V + v$, taking $u, v, w \ll V$ and neglecting terms of second and higher order in u, v , and w , we obtain

$$\frac{V}{r} \frac{\partial u}{\partial \lambda} - v \left(f + \frac{2V}{r} \right) = K \frac{\partial^2 u}{\partial z^2}$$

$$\frac{V}{r} \frac{\partial v}{\partial \lambda} + u \left(f + \frac{V}{r} + \frac{\partial V}{\partial r} \right) = K \frac{\partial^2 v}{\partial z^2}, \quad (5)$$

which is linear in (u, v) . In the limit $r \rightarrow \infty$, this reduces to the classic Ekman equations in Cartesian coordinates.

Equation (5a) represents the radial flow balance between accelerations due to azimuthal advection, gradient wind imbalance, and turbulent transport. The second represents the balance for the azimuthal component, between the azimuthal and radial advection of absolute angular momentum, and its turbulent transport. This linearization will not be valid in the case of an inertially neutral storm, when the coefficient of u in (5b) will

become 0, and other processes will have to balance the turbulent transport of v . This case will be explored in Part II. Note that Smith (1968) commented that the removal of vertical advection is not supported by scale analysis. In particular, for a symmetric vortex within the radius of maximum inflow, the continuity equation gives $W/H \sim V/R$, where W and V are scales for vertical and horizontal velocity, and H and R are vertical and horizontal length scales. Then the vertical advection terms in (4) scale as $WV/H \sim V^2/R$, which is the same order as other terms retained in (5). This will later be shown to be one of the major sources of differing predictions by this linear model, and the numerical model in Part II. Nevertheless, as the linear model will be seen to contain useful physical insight, we will persevere with it.

We write (5) as

$$2\gamma \frac{\partial \omega}{\partial \lambda} + 2i\sqrt{\alpha\beta}\omega - \frac{\partial^2 \omega}{\partial z^2} = 0, \tag{6}$$

where we have combined u and v into the complex variable

$$\omega = \sqrt{\frac{\beta}{\alpha}}u + iv \quad \text{and} \tag{7}$$

$$\alpha = \frac{1}{2K} \left(f + \frac{2V}{r} \right) \quad \beta = \frac{1}{2K} \left(f + \frac{V}{r} + \frac{\partial V}{\partial r} \right) \tag{8}$$

$$\gamma = \frac{1}{2K} \frac{V}{r}.$$

We expand (6) as a Fourier series in azimuth,

$$\omega(\lambda, z) = \sum_{k=-\infty}^{\infty} a_k(z)e^{ik\lambda}, \tag{9}$$

for complex coefficients $a_k(z)$, whence

$$\sum_{k=-\infty}^{\infty} [2i(\gamma k + \sqrt{\alpha\beta})a_k(z) - a_k''(z)]e^{ik\lambda} = 0. \tag{10}$$

Equating coefficients of $\exp(ik\lambda)$ to zero gives a family of second-order ordinary differential equations in $a_k(z)$. Seeking solutions $a_k(z) = A_k \exp(p_k z)$ for some constants A_k and p_k , we find

$$p_k = \pm(1 + i)(\sqrt{\alpha\beta} + k\gamma)^{1/2}. \tag{11}$$

We immediately eliminate the solution with positive real part, as we require the perturbations u and v to go to zero as $z \rightarrow \infty$. We will write the required root as

$$p_k = \begin{cases} -(1 + i)(\sqrt{\alpha\beta} + k\gamma)^{1/2}, & \sqrt{\alpha\beta} + k\gamma > 0 \\ -(1 - i)(|k|\gamma - \sqrt{\alpha\beta})^{1/2}, & \sqrt{\alpha\beta} + k\gamma < 0. \end{cases} \tag{12}$$

For clarity, we will always write equations so that only positive real numbers appear under square root signs and thus avoid the potential confusion of deciding which

complex square root to take. While the former case will prevail in the cyclone core for low wavenumbers $|k|$, the latter can occur anywhere for sufficiently large negative k but may occur outside the core even for $k = -1$, in storms with a moderately peaked radial wind profile and hence weak relative vorticity. The implications of this change of sign will be discussed further below. In the intermediate case $(\alpha\beta)^{1/2} + k\gamma = 0$, both roots are zero.

The usual approach to solving the Ekman equations uses a noslip lower boundary condition, $u(0) = 0, v(0) = -V$. This does not well represent atmospheric conditions and also grossly violates the linearization here. Instead, we will apply a slip condition near the surface, and use a bulk formulation with drag coefficient C for the near-surface stress,

$$K \frac{\partial u}{\partial z} = C\sqrt{(u + u_t)^2 + (V + v + v_t)^2}(u + u_t)$$

$$K \frac{\partial v}{\partial z} = C\sqrt{(u + u_t)^2 + (V + v + v_t)^2}(V + v + v_t), \tag{13}$$

evaluated at some height in the surface layer, which for convenience we will take to be $z = 0$. Here, (u_t, v_t) is the cyclone translation velocity, which we will take as being in the positive x direction with speed U_t , giving

$$u_t = \frac{1}{2}U_t(e^{i\lambda} + e^{-i\lambda}) \quad v_t = \frac{i}{2}U_t(e^{i\lambda} - e^{-i\lambda}). \tag{14}$$

We assume that $U_t \ll V$, and linearize (13):

$$CV(u(0) + u_t) = Ku'(0)$$

$$CV(V + 2v(0) + 2v_t) = Kv'(0). \tag{15}$$

As this cannot be written as an algebraic function of ω , it is necessary to separate out the real and imaginary parts of (10), giving

$$\text{Re} \left\{ \sqrt{\frac{\alpha}{\beta}} \sum_{k=-\infty}^{\infty} A_k \left[\frac{CV}{K} + (1 + i)(\sqrt{\alpha\beta} + k\gamma)^{1/2} \right] e^{ik\lambda} + \frac{1}{2} \frac{CV}{K} U_t (e^{i\lambda} + e^{-i\lambda}) \right\} = 0$$

$$\text{Im} \left\{ \sum_{k=-\infty}^{\infty} A_k \left[\frac{2CV}{K} + (1 + i)(\sqrt{\alpha\beta} + k\gamma)^{1/2} \right] e^{ik\lambda} + \frac{CV}{K} (U_t(-e^{i\lambda} + e^{-i\lambda}) + iV) \right\} = 0. \tag{16}$$

A little care is needed in solving (16). Since we have taken real and imaginary parts, we can no longer simply equate coefficients of powers of $\exp(ik\lambda)$ to 0. One route is to substitute in some suitable values for λ and solve the resulting system of equations. A more elegant approach is to use the identities $\text{Re}(z) = (z + z^*)/2, \text{Im}(z)$

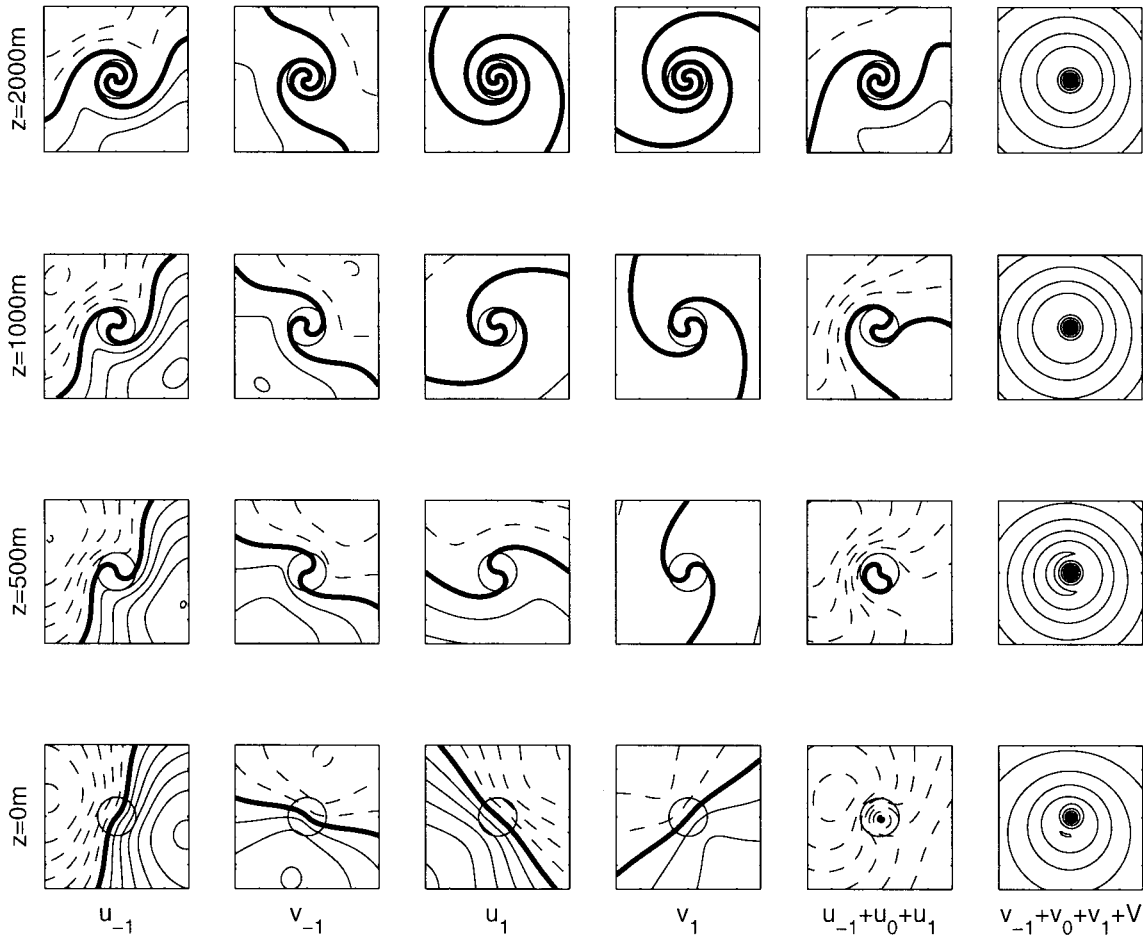


FIG. 3. The two components of the asymmetric flow, (u_{-1}, v_{-1}) (left two columns) and (u_1, v_1) (middle two columns), together with the total storm-relative radial and azimuthal flow (last two columns) at the surface (bottom row), 500 m (second from bottom), 1 km (second top), and 2 km (top), for the cyclone in Fig. 2, moving to the west at 5 m s^{-1} . The central circles in all except the last column show the maximum wind belt, and the domains are each 300-km square. The contour interval is 1 m s^{-1} in the first two columns, 0.25 m s^{-1} in the next two, 2 m s^{-1} in the fifth, and 5 m s^{-1} in the last. Negative contours are dashed, and the zero contour is bold.

$= i(-z + z^*)/2$, where z^* is the complex conjugate of z , to eliminate the Re and Im functions. The coefficients of $\exp(ik\lambda)$ in the pair of equations thus obtained from (16) must then be 0. This gives a system of linear equations in A_k and A_k^* , which we solve. For $|k| \geq 2$, $A_k = 0$, since in a linear model there is nothing to excite wavenumbers above 1. For $|k| \leq 1$ and $(\alpha\beta)^{1/2} - \gamma > 0$,

$$\begin{aligned}
 A_1 &= -\frac{\eta[1 - 2\sqrt{\alpha/\beta} + (1 + i)(1 - \sqrt{\alpha/\beta})\psi]U_i}{\sqrt{\alpha/\beta}(2 + 2i)(1 + \eta\psi) + 3\eta + 3i\psi} \\
 A_0 &= -\frac{\chi[1 + i(1 + \chi)]V}{2\chi^2 + 3\chi + 2} \\
 A_{-1} &= -\frac{\psi[1 + 2\sqrt{\alpha/\beta} + (1 + i)(1 + \sqrt{\alpha/\beta})\eta]U_i}{\sqrt{\alpha/\beta}(2 + 2i)(1 + \eta\psi) + 3\psi + 3i\eta},
 \end{aligned}
 \tag{17}$$

where

$$\begin{aligned}
 \eta &= \frac{CV}{K(\sqrt{\alpha\beta} + \gamma)^{1/2}} = CV\sqrt{\frac{2}{K(V/r + I)}} \\
 \chi &= \frac{CV}{K(\alpha\beta)^{1/4}} = CV\sqrt{\frac{2}{KI}} \\
 \psi &= \frac{CV}{K(|\sqrt{\alpha\beta} - \gamma|)^{1/2}} = CV\sqrt{\frac{2}{K|V/r - I|}}
 \end{aligned}
 \tag{18}$$

are dimensionless numbers, and $I^2 = (f + 2V/r)(f + V/r + \partial V/\partial r)$ is the square of the inertial stability. For $(\alpha\beta)^{1/2} - \gamma < 0$, a slightly different form is obtained for the asymmetric components¹

¹ If we replace ψ by $-i\psi$ for A_1 and by $i\psi$ for A_{-1} in (17), then (19) is obtained.

$$\begin{aligned}
 A'_1 &= -\frac{\eta[1 - 2\sqrt{\alpha/\beta} + (1 - i)(1 - \sqrt{\alpha/\beta})\psi]U_i}{\sqrt{\alpha/\beta}[2 + 2i + 3(\eta + \psi) + (2 - 2i)\eta\psi]} \\
 A'_{-1} &= -\frac{\psi[1 + 2\sqrt{\alpha/\beta} + (1 + i)(1 + \sqrt{\alpha/\beta})\eta]U_i}{\sqrt{\alpha/\beta}[2 - 2i + 3(\eta + \psi) + (2 + 2i)\eta\psi]}
 \end{aligned}
 \tag{19}$$

using A' instead of A to avoid ambiguity.

The boundary layer flow is thus given by

$$\begin{aligned}
 u(\lambda, z) &= u_1(\lambda, z) + u_0(z) + u_{-1}(\lambda, z) \\
 v(\lambda, z) &= v_1(\lambda, z) + v_0(z) + v_{-1}(\lambda, z),
 \end{aligned}
 \tag{20}$$

where u_0 and v_0 are, respectively, $(\alpha/\beta)^{1/2} = [(f + 2V/r)/(f + V/r + \partial V/\partial r)]^{1/2}$ times the real part, and the imaginary part, of

$$\omega_0(z) = A_0 \exp\left(-\frac{(1 + i)z}{\delta_0}\right).
 \tag{21}$$

The asymmetric components (u_1, v_1) and (u_{-1}, v_{-1}) are similarly obtained from

$$\begin{aligned}
 \omega_1(\lambda, z) &= \begin{cases} A_1 \exp\left(-\frac{(1 + i)z}{\delta_1} + i\lambda\right), & I > V/r \\ A'_1 \exp\left(-\frac{(1 + i)z}{\delta_1} + i\lambda\right), & I < V/r \end{cases}
 \end{aligned}
 \tag{22}$$

and

$$\begin{aligned}
 \omega_{-1}(\lambda, z) &= \begin{cases} A_{-1} \exp\left(-\frac{(1 + i)z}{\delta_{-1}} - i\lambda\right), & I > V/r \\ A'_{-1} \exp\left(-\frac{(1 - i)z}{\delta_{-1}} - i\lambda\right), & I < V/r. \end{cases}
 \end{aligned}
 \tag{23}$$

The depth scales of the three components are

$$\delta_k = \frac{1}{(|\sqrt{\alpha\beta} + k\gamma|)^{1/2}} = \sqrt{\frac{2K}{|I + kV/r|}}.
 \tag{24}$$

The solutions [(22), (23)] are continuous at those isolated points where $I = V/r$, if such points exist, although the radial gradients become large. The behavior there will be discussed further below.

The frictionally induced agradient flow has thus been decomposed into three components. The two components with azimuthal wavenumber 1 are proportional to the translation speed U_i , while the symmetric component is proportional to the gradient wind speed V . Each solution has a different depth scale δ_k , which is longest for $k = -1$, and shortest for $k = 1$. A physical explanation for these different length scales is given later. Note that because of the linearization of the surface

boundary condition in (15), and particularly the assumption $U_i \ll V$, the asymmetric parts of the solution do not reduce to the Ekman limit for straight flow far from the vortex, although the symmetric part does. In fact, as $r \rightarrow \infty$, each of A_0/V^2 , $A_1/(VU_i)$ and $A_{-1}/(VU_i)$ approach nonzero constants, so each of the $(u_k, v_k) \rightarrow 0$. However, in reality, the asymmetric components should become proportional to U_i^2 then, and so are valid only in that part of the vortex where $V \gg U_i$. Note also that the limiting behavior $A_0 \sim V^2$ for small V follows from the slip boundary condition, rather than the circular geometry. Exactly the same behavior arises when the classical Ekman equations in Cartesian coordinates are solved with this boundary condition.

We now consider separately the symmetric and asymmetric components of the solution with a particular focus on the low-level jet in tropical cyclones.

3. The boundary layer of a stationary vortex

Here, only the symmetric part (u_0, v_0) of the solution applies. It differs from the classical Ekman spiral in three ways. The first is that the depth scale is $\delta_0 = (2K/I)^{1/2}$, rather than $(2K/f)^{1/2}$. In the core of a tropical cyclone, this is much less. The effect of storm rotation in reducing the depth of the boundary layer has been noted before, for example by Eliassen and Lystad (1977), Anthes and Chang (1978), and Frank (1984), the latter two of whom took the depth as being proportional to $(f + 2V/r)^{-1/2}$. The analysis here, which will be confirmed by the numerical modelling results in Part II, suggests that $(2K/I)^{1/2}$ is a more appropriate scale.

The second important difference is that the square root term in (7) alters the degree of turning of wind direction with height from the classic solution. Inside the eye of a cyclone, this term will be close to 1. However, outside the eye, V/r and $\partial V/\partial r$ have opposite signs and will partially cancel, leading to a stronger cross-isobar component, relative to the along-isobar component, than in the solution for straight flow. This will become more marked as the inertial stability of the storm decreases toward neutrality, until at the neutral limit, $\beta = 0$, and the model ceases to be valid. Further, the change in sign of $\partial V/\partial r$ at the radius of maximum winds will produce a marked gradient in the near-surface inflow there, and hence substantial near-surface convergence. The vertical velocity forcing implied by this solution will be discussed in detail below.

The final important difference lies in the coefficient A_0 , which affects the phase and amplitude of the spiral. This is different because of both the slip boundary condition, and our arbitrary definition of $z = 0$ as being some height in the surface layer, rather than the actual surface. While the first two of the differences noted here are due to the application to a vortex, this latter one is rather a consequence of the surface boundary condition. Indeed, the solution for horizontally homogeneous geostrophically balanced straight flow in Cartesian coor-

dinates, with this slip boundary condition, may be recovered from (21) by replacing I by f in the definition (18) of χ , and setting the coefficient $(\alpha/\beta)^{1/2}$ used in extracting u from (21) equal to 1.

The variation of the dimensionless parameter χ with wind speed is clearly of interest. Unfortunately, determining this is not easy, as C , K , and I will each vary with V . Of these, the turbulent diffusivity is perhaps the most difficult dependence to assign. One possibility is to take the turbulence length scale as proportional to height, on the grounds that the turbulence is predominantly shear generated. Thus a representative length scale for the whole boundary layer, as required here, is the boundary layer depth δ_0 , and the diffusivity can be parameterized as

$$K \sim (\text{turbulent length scale})^2 |\text{shear}| \sim \delta_0^2 \frac{V}{\delta_0} \\ = \delta_0 V. \quad (25)$$

Substituting this and the definition of δ_0 into (18b), we find that $\chi \sim C$. The linear increase of C with wind speed, at least up to 25 m s^{-1} , is well documented (e.g., Garratt 1977; Large and Pond 1981), although there is some disagreement about whether this increase is maintained at higher speeds (e.g., Frank 1984; Hubbert et al. 1991). We may also substitute (25) into (24) to find

$$\delta_0 \sim \frac{V}{I}, \quad (26)$$

removing the dependence on turbulence parameters. This result, while potentially useful, relies on a scaling argument for the turbulence parameters, and so should be used with caution. We will investigate this point further in Part II.

The height and strength of the maximum azimuthal wind may be found by solving $v'_0(z) = 0$, giving

$$z_{\max} = \delta_0 \arctan(-1 - 2/\chi) \\ v(z_{\max}) = V \frac{e^{-\arctan(-1-2/\chi)} \chi \sqrt{\chi^2 + 2\chi + 2}}{\sqrt{2} (2\chi^2 + 3\chi + 2)}. \quad (27)$$

Values for the arctangent function here lie in the range $\pi/2$ to $3\pi/4$, so the precise details of the storm can vary the height of the jet by about 50% within our scale estimate of δ_0 . Note here that an inertially more neutral storm will have a higher jet, through both δ_0 and the arctan term, and that increasing the drag coefficient will lower the jet. Remarkably, the strength of the jet relative to the gradient flow is expressed entirely in terms of χ . Figure 1 shows the effect of individually varying the five of six parameters (diffusivity, drag coefficient, gradient wind speed, radius, and inertial stability)—the effect of varying latitude is, unsurprisingly, negligible through a physically reasonable range, on jet height and relative strength. Here the inertial stability is parameterized through a variable x , defined by $\partial V/\partial r = xV/r$,

and the parameters are varied about the values $K = 50 \text{ m}^2 \text{ s}^{-1}$, $C = 0.002$, $V = 40 \text{ m s}^{-1}$, $f = 3.77 \times 10^{-5} \text{ s}^{-1}$ (for latitude 15°), $r = 40 \text{ km}$, and $x = -0.5$ (Gray and Shea 1973).

The jet in this linear model is substantially weaker than in the observations, being typically from 2% to 4% supergradient. We will argue below and confirm in Part II that this is a consequence of the linear model, and that incorporating the vertical advection in particular, produces a result more consistent with the observations.

An interesting feature of Fig. 1 is that increasing the drag coefficient (over the range given) markedly increases the jet strength, with only a minor effect on the height. This is because greater surface friction leads to stronger inflow through much of the boundary layer, and hence greater inwards advection of angular momentum. This is potentially important, because of both the poorly known wind speed dependence of the drag coefficient at high winds, and the marked increase that (usually) occurs at landfall. The timescale for the boundary layer to develop was shown by Eliassen and Lystad (1977) to be $1/I$, and is less than an hour for the inner part of a hurricane. This therefore suggests that the jet will strengthen at, or soon after, landfall.

Increasing gradient wind speed is seen to lead to a shallower, stronger jet, although we caution that in the real atmosphere stronger winds would be expected to lead also to an increase in turbulent diffusivity and drag coefficient. The increase in K would tend to reverse this trend, while the increase in C would further increase the strength, but slightly increase the height.

Varying the radius alters the inertial stability, leading to a lower but weaker jet for a more compact storm, all other things being equal. Finally, the effect of varying the radial profile of gradient wind is that, in a more peaked, inertially neutral storm, x will be closer to -1 , giving a stronger but higher jet. We see also that just inside the radius of maximum winds, where x is positive, the jet is predicted to be lower and weaker than just outside. Note that care is needed in interpreting this last pair of panels for in-eye conditions as the gradient wind speed is held constant for them.

a. Vertical velocity forcing in a stationary vortex

The vertical velocity above the boundary layer can be found by integrating the continuity equation vertically and applying the surface boundary condition $w = 0$, giving

$$w_\infty(r) = -\frac{1}{r} \frac{\partial}{\partial r} \left(r \int_0^\infty u \, dz \right) \\ = \frac{1}{r} \frac{\partial}{\partial r} \left\{ \frac{rCV[V + 2v(0)]}{f + V/r + \partial V/\partial r} \right\}. \quad (28)$$

Here, we have used (5b) and (15b) to write

$$\begin{aligned}
 2\beta \int_0^\infty u(z) dz &= \int_0^\infty v''(z) dz = v'(\infty) - v'(0) \\
 &= -\frac{CV}{K}(V + 2v(0)) \quad (29)
 \end{aligned}$$

in a stationary vortex. A similar result was found by Eliassen and Lystad (1977). This is in several respects an interesting result. First, it is nearly independent of K —only the weak influence through $v(0)$ remains. Second, if we neglect the radial variation of $f + V/r + \partial V/\partial r$ in (32), we see that the Ekman pumping velocity is proportional to the curl of the surface stress, as in the classical solution. Neglecting the radial gradient of vorticity will not introduce large errors, except near the eyewall, where it is obviously significant and would result in a markedly stronger updraft. Finally, if we assume that $v(0)$ is proportional to V , it is easy to consider three particular cases.

- *Solid body rotation* $V = \Omega r$, and w_∞ is proportional to r ; that is, frictional forcing produces ascent proportional to radius in the eye. This result was also obtained by Eliassen (1971) and Eliassen and Lystad (1977).
- *Rankine vortex* $dV/dr = -V/r$, and w_∞ is proportional to $-1/r^3$ and we have subsidence increasing rapidly toward the center of the storm. Thus storms with a highly peaked wind profile will be subsident outside the radius of maximum winds (RMW), although we caution here that we are approaching the limits of applicability of the linear model. The subsidence here is quite different to the predictions of the standard Ekman model for this case, which predicts zero vertical velocity from the irrotational gradient level flow. However, Carrier (1971, see footnoted correction due to J. McWilliams) found subsidence proportional to r^{-2} in a similar vortex. The weaker radial dependence is due to their use of a no-slip boundary condition.
- *Typical cyclone* with V proportional to r^{-x} and $x \approx 1/2$, and also $\partial V/\partial r + V/r \gg f$. This gives w_∞ proportional to r^{-x} and hence to V , and upward.

Comparing the latter two of these cases with the first confirms that the maximum updraft must lie in the vicinity of the rmw. Determining the precise location is somewhat more difficult. The cases considered by Eliassen and Lystad (1977) all had the maximum updraft inside the radius of maximum winds. However, when we calculate the updraft for the parametric wind profile of Holland (1980) below, the maximum updraft above the boundary layer lies slightly outside the radius of maximum winds. We show in the appendix that the difference is due to the relatively weak vortices considered by Eliassen and Lystad (1977). They also found in their numerical results that the location of the maximum updraft moved inward as the drag coefficient increased. This phenomenon is also explained in the appendix, and shown to be unlikely to be important in real

tropical cyclones. We discussed earlier that a limitation of the linear model is that the neglect of vertical advection is not supported by a scale analysis. This shortcoming can thus be expected to be most serious near the rmw, and will be shown to be so in Part II.

b. Surface wind reduction

Consider for simplicity the ratio of surface azimuthal wind, rather than surface wind speed, to gradient wind. This is substantially different only in the nearly inertially neutrality case, when the model is at the limits of its validity anyway. Then the surface wind factor is

$$\frac{V + v(0)}{V} = \frac{\chi^2 + 2\chi + 2}{2\chi^2 + 3\chi + 2}, \quad (30)$$

which decreases monotonically from 1 at $\chi = 0$ to a limiting value of $1/2$ as $\chi \rightarrow \infty$. Reasonable values of the parameters (near the eyewall, $C = 0.002$, $V = 40 \text{ m s}^{-1}$, $K = 50 \text{ m}^2 \text{ s}^{-1}$, and $I = 10^{-3} \text{ s}^{-1}$) give a factor of 0.81, which is consistent with the studies cited earlier. At larger radii, if the radial variation in χ is indeed similar to that for C as suggested earlier, then relatively weaker surface winds will be found. The observational studies cited earlier have shown that there is no universal constant surface wind factor, and have tended to ascribe the differences to stability effects. Here, we have shown that dynamical factors play a substantial role.

c. Application to a typical cyclone

The above may readily be applied to any of the several analytical wind profiles in the literature. We adopt that of Holland (1980), since it is in a form which enables easy adjustment of the storm intensity, maximum wind radius, and shape of the wind profile outside the radius of maximum winds, and it satisfies known constraints on radial variation of angular momentum. In addition, it has been widely used and received considerable verification against observations, both in the original paper and subsequently (e.g., Harper et al. 1989, 1993). The profile within the eye is slightly modified to remove the barotropic instability present there. This is not strictly necessary here, but will be for Part II, and so is adopted here for consistency. The details are given in Part II.

Figure 2a shows the radial profiles of gradient wind from the Holland profile, and “surface” wind speed components from the linear model here, for a cyclone with maximum wind speed 40 m s^{-1} at a radius of 40 km. The Holland b parameter, which controls the radial velocity gradient and hence the inertial stability outside the radius of maximum winds, is 1.3, which is an average value for tropical cyclones. The inflow is seen to increase inward more slowly than the azimuthal wind, before decreasing again inside the radius of maximum winds. The surface azimuthal wind is about 77% of the gradient wind outside the rmw, but relatively much stronger at and inside of the rmw (Fig. 2e). This follows

through (30) from the radial variation of χ , which is nearly constant outside the rmw, where V and $I^{1/2}$ have similar radial tendencies, but decreases rapidly to 0 at the center, as V decreases and $I^{1/2}$ remains large.

The jet strength (Fig. 2c) is quite weak, about 3% supergradient, outside the rmw, decreasing rapidly inside the eye, while its height (Fig. 2d) decreases nearly linearly towards the centre. Vertical velocity at three levels is shown in panel b; the peak at the rmw and approximately linear dependence inside are apparent, as predicted in the discussion above. An exact linear dependence is not found because our gradient wind profile does not have a linear dependence here. It is interesting that the radial profiles of w at 200 and 500 m are much more peaked than the one for the limit as $z \rightarrow \infty$, and that the updraft slopes outwards with height. This is partly a reflection of the shallower boundary layer towards the center, but also that the radius of maximum inflow tilts outward with height. In fact, as was pointed out by Rosenthal (1962), the radius of maximum horizontal convergence lies just within the rmw at the surface, but increases steadily with height as radius increases, to approximately 1500 m at a radius of 150 km. Thus the lower boundary layer flow at large radii is accelerating inward, and so there is comparatively weak low-level convergence there.

Figure 2f shows the diffusive forcing of inflow $K\partial^2 u/\partial z^2$ at the jet height. In the present model, this is all that balances the outward acceleration due to gradient wind imbalance. In the real atmosphere, inflow is additionally forced by vertical advection $-w\partial u/\partial z$, shown dashed in panel f. This is comparable to the diffusive forcing, and had it been included in the model, a more strongly supergradient flow could have been maintained in the upper boundary layer. Thus the present model underestimates the jet strength in the core region. Note that this argument is indicative rather than quantitative, as the vertical velocity field would be different in a nonlinear model. This and the other nonlinear terms are considered in detail in Part II.

4. The boundary layer in a moving cyclone

Each of the azimuthal wavenumber 1 components in the agradient flow varies in height as an exponentially decaying sinusoid. The decay and oscillation depth scales δ_1 and δ_{-1} are respectively shorter and longer than the symmetric component's scale, δ_0 . The phase of each component rotates with height. For (u_1, v_1) , the imaginary parts of the coefficients of z and λ in the argument to the exponential function in (22) have opposite signs, so the phase rotates cyclonically with height. Similarly, from (23), the phase of (u_{-1}, v_{-1}) rotates anticyclonically where $I > V/r$, and cyclonically where $I < V/r$. The rate of rotation depends on the governing height scale, so it is always quicker for (u_1, v_1) than (u_{-1}, v_{-1}) , and is also quicker in the inertially highly stable core of the cyclone. Approaching the limit

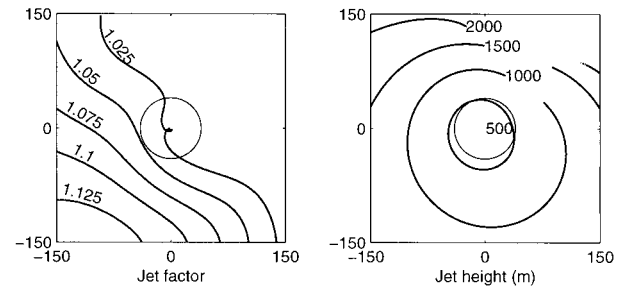


FIG. 4. Jet strength, (using earth-relative winds; left) and height (right), for the storm in Fig. 3. The central circles and vertical lines show the radius of maximum winds. Contours of jet height are discontinuous in the rear right quadrant of the storm, as there is no jet there.

$I = V/r$ from either side, the components become equal and constant with height, which corresponds to the double root $p_k = 0$. Physically, this is a surprising result, as it suggests that this component of the flow does not suffer frictional retardation. However, we point out that the other two components are retarded, and that this one scales as the cyclone translation speed, which we have necessarily assumed is much less than the gradient wind speed. Thus the absence of shear in this component is not unrealistic. A physical interpretation of the differing phase rotation with height and depth scales, will be given below.

Figure 3 shows the components of the asymmetric and total storm-relative flow at several heights, for the same cyclone as in Fig 2, translating to the west at 5 m s^{-1} . Clearly (u_{-1}, v_{-1}) is several times stronger, and decays and rotates less rapidly with height, than (u_1, v_1) . Inside the eye, where I is large and greater than V/r , both components have similar and relatively rapid rates of rotation with height, although in opposite directions.

The asymmetric part of the flow is dominated by (u_{-1}, v_{-1}) , and consists of inflow in the right forward quadrant, and outflow in the left rear, in good agreement with observational studies (Shea and Gray 1973; Frank 1984). Above 1 km in the right rear quadrant, the asymmetric outflow component u_{-1} dominates the symmetric inflow component u_0 , due to its slower decay with height, giving a significant area of net outflow. This appears similar to the strong outflow found by Marks et al. (1999) to the rear of Hurricane Fran. Interestingly, there are two small regions near the surface where u_{-1} exceeds the translation speed U_t .

The asymmetry in the azimuthal flow gives a maximum on the left side near the surface in the total storm-relative flow, rotating towards the front with increasing height, due to the rotation with height of the dominant asymmetric term v_{-1} . The other term, v_1 , makes a noticeable contribution only very near the surface. Again, this azimuthal flow is in reasonable agreement with the previously cited observational studies.

The effect of the asymmetries on the jet for the same

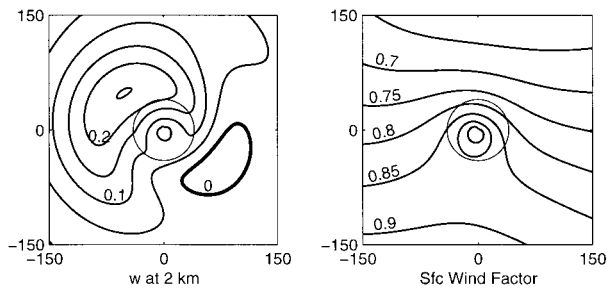


FIG. 5. Vertical velocity (left), and surface wind reduction factor (using earth-relative winds; right), for the same storm as in Fig. 3.

storm are shown in the upper panels of Fig. 4. The jet is strengthened in the left front quadrant where the asymmetric component v_{-1} is positive, and obliterated in the right rear. Here, the “jet factor” is defined as the ratio of the wind speed at the jet core to the gradient wind, in an earth-relative coordinate system. The asymmetry in height is less marked, particularly in the core when the jet is nearer the surface. This is because the bulk of the vertical variation in wind is explained by the symmetric part of the solution, with the asymmetric parts either being much weaker in the case of (u_1, v_1) , or varying over a substantially longer depth scale in the case of (u_{-1}, v_{-1}) . In either case, they produce weaker vertical shear than the symmetric component. Thus the height of the jet, where it still exists, is not dramatically modified from the symmetric case.

The effect of translation on the vertical velocity and surface wind factor are shown in Fig. 5. Above the boundary layer, the wavenumber 1 asymmetry induces an enhanced updraft in the right forward quadrant, while eliminating the updraft at the left rear. The weak anticyclonic spiral in the updraft is a consequence of the dominant asymmetric (u_{-1}, v_{-1}) component. It is clearly not a forcing for spiral bands, but may be partly responsible for observed eyewall asymmetries. There is a broad left–right gradient of surface wind reduction factor, with larger values on the weaker side of the storm, as well as the enhanced values near the centre noted above. This left–right asymmetry does not seem to have been previously noted, and is another possible dynamical explanation for the aforementioned variation in observed surface wind reduction factors.

a. Physical interpretation of the asymmetries

If the time derivative is restored and the friction terms removed from the original linear equations (5), the resulting system has an infinite family of inertia waves as solutions, given (to within arbitrary phase and amplitude) by

$$\begin{aligned}
 u(t, \lambda) &= \sqrt{\frac{f + 2V/r}{f + V/r + \partial V/\partial r}} \cos \left[\left(I + \frac{Vk}{r} \right) t - k\lambda \right] \\
 v(t, \lambda) &= -\sin \left[\left(I + \frac{Vk}{r} \right) t - k\lambda \right].
 \end{aligned} \quad (31)$$

For the case of interest $|k| = 1$, these have phase angular velocity $V/r \pm I$; that is, I in either direction, Doppler shifted by the cyclone’s gradient flow. We will dub these the “fast” and “slow” waves, depending on whether they are propagating with or against the flow, respectively. The fast wave always travels cyclonically, while the slow wave will propagate anticyclonically in the inertially highly stable cyclone core, but may go the other way or be stationary in regions of weak inertial stability.

Although supported by the linearised inviscid equations of motion, the waves probably have little physical significance as they stand. For instance, their phase angular velocity is a strong function of radius, so the radial phase relationship will vary with time. Moreover, the wave (31) is divergent, and the pattern of divergence has a complex time evolution due to the radial variation of angular velocity, but the associated mass changes have been eliminated by the linearization. Rather, the importance of these waves is to the physical interpretation of the two asymmetric components. We now show that in the viscous case, the vertical structure of these waves is such that friction brings them to a halt.

These waves have the same azimuthal structure as the solution components (u_1, v_1) and (u_{-1}, v_{-1}) . The friction $K\partial^2/\partial z^2$ term is always in quadrature with the velocity field, and lagging, relative to the direction of propagation of the corresponding wave. Thus friction can only retard the waves, and not change their amplitude.

Moreover,

$$\begin{aligned}
 \frac{\text{amplitude}(u_1)}{K \text{amplitude}(\partial^2 u_1/\partial z^2)} &= I + \frac{V}{r}, \\
 \frac{\text{amplitude}(u_{-1})}{K \text{amplitude}(\partial^2 u_{-1}/\partial z^2)} &= \left| I - \frac{V}{r} \right|,
 \end{aligned} \quad (32)$$

and similar relationships apply for the v components. This, in combination with the quadrature phase relationships, shows that precisely enough friction is present to retard the wave to stationarity. In the case where $I = V/r$, the wave is already stationary, no retardation of the wave is required, and so no vertical shear is present in (u_{-1}, v_{-1}) .

Now (u_1, v_1) corresponds to the fast wave, and thus requires relatively more friction to stop it, than (u_{-1}, v_{-1}) . Hence the former has both a shorter vertical length scale, giving relatively stronger shear, and a lower amplitude, than the latter. Moreover, since K is constant here, and the amplitude of each wave decreases with height, it is easy to see that the vertical stress divergence can only lag the wave in phase if the phase of the wave rotates with height in the same direction as it would have propagated in the absence of friction. Thus the phases of (u_1, v_1) and (u_{-1}, v_{-1}) will generally rotate in opposite directions, with height.

5. Summary and conclusions

Many observed wind profiles within the tropical cyclone boundary layer show a low level maximum. A linear analytical model of the tropical cyclone boundary layer was presented and used to diagnose the properties of, and deduce the dynamics causing, this low-level jet. This model diagnoses the boundary layer flow as the frictional response to an imposed, prescribed gradient flow characteristic of a cyclone, ignoring the feedback from boundary layer processes onto the cyclone as a whole, and thus represents one side of what is undoubtedly a two-way interaction. The solution bears some resemblance to the well-known Ekman boundary layer model. However, it has three components, the first being a symmetric one due to the cyclone, and two asymmetric ones resulting from the interaction of the moving cyclone with the underlying surface. Each has a different depth scale, which are each different to that of the classical Ekman solution. There is also an asymmetry between the radial and azimuthal components of the flow not present in the classic solution, which makes the radial component relatively stronger than the azimuthal in all three components. The symmetric component is an extension of the symmetric vortex models of Rosenthal (1962) and Eliassen and Lystad (1977), while the asymmetric solution is believed to be new.

It was shown that strong inwards advection of absolute angular momentum was necessary to produce the jet. In the linear model, this inflow was maintained against gradient adjustment by vertical diffusion, and the wind maximum was found to be a few percent supergradient in a stationary cyclone. It was argued that the vertical advection term should be of similar size, and that therefore the jet strength is substantially underestimated here. Further, since enhanced inflow into the outer side of a rainband and a stronger radial gradient of M_a will give stronger advection of M_a there, and that there is an increased updraft, we speculate that this may be a favored location for jets.

The jet height was predicted to scale as $\delta_0 = (2K/I)^{1/2}$. It was argued that the introduction of vertical advection to the linear model would not bring any new height scales, and so this should also apply approximately in a full nonlinear model.

The Ekman spiral is nowadays generally regarded as a fairly poor model of the atmospheric boundary layer, yet here a related model is advanced as being appropriate in tropical cyclones. We suggest it is valid, because several of the factors that commonly disturb the classical Ekman spiral will apply to a much lesser degree in the tropical cyclone boundary layer. The first of these, the nonslip boundary condition, is here replaced by one of several possible slip conditions.

Second is the role of buoyancy in generating turbulence. In the strongly sheared environment of the tropical cyclone boundary layer, turbulence would be expected to be dominantly shear-generated. This would

lead to a relatively simple turbulent diffusivity structure, not subject to large diurnal variations. As the timescale $1/f$ for the establishment of an Ekman spiral is similar to the time over which diurnally induced variations in diffusivity occur, it is perhaps hardly surprising that it is rarely observed over the land. Indeed, it is worth noting that Taylor (1914), in his comparison of aircraft data to an Ekman spiral (with a slip boundary condition), restricted attention to the strong wind case for precisely this reason.

Another factor that can eliminate or even reverse the turning of the winds in the boundary layer is baroclinicity. This would be less important in a tropical cyclone, as the near-surface temperature gradients are weak and tend to be aligned perpendicular to the flow. Moreover, the altered scaling that results in a markedly shallower boundary layer here also reduces the extent to which temperature gradients can contribute to significant shear across the boundary layer.

A final factor which, in contrast to the others, does apply in the tropical cyclone boundary layer, is the hydrodynamic instability of the Ekman spiral. For instance, the numerical studies of Faller and Kaylor (1966) and Lilly (1966), and the analytical work of Brown (1970, 1972a,b), show that the classical Ekman spiral is unstable and breaks down into longitudinal rolls, aligned at approximately 14° to 17° to the geostrophic flow. Longitudinal rolls are well known to occur in the atmospheric boundary layer, and recently some evidence of their occurrence in the tropical cyclone boundary layer has appeared (Wurman and Winslow 1998).

Is the jet, then, nothing more than the weakly supergradient flow found near the top of the Ekman boundary layer? In the context of the linear model, the answer is essentially yes; albeit with the complication of three separate components in a moving storm. However, we indicated here, and will confirm in Part II using a numerical model, that vertical advection plays a crucial role in strengthening the jet, and that the supergradient component may be several times stronger than is predicted by the linear model. The major role of upward advection seems to be peculiar to intense vortices and does not occur in more normally considered cases. This is because the rapid, almost steplike increase in inertial stability near the radius of maximum winds produces an updraft that is much stronger than would be expected from the classical theory, in which the updraft is proportional to the curl of the surface stress.

It was also shown that the distribution of vertical velocity outside the core region may not follow the predictions of the classical Ekman theory, as surface divergence may prevail even in the presence of cyclonic relative vorticity, provided the inertial stability is weak. Within the eye, the updraft is proportional to radius, in agreement with the results of Eliassen (1971) and Eliassen and Lystad (1977).

For a moving storm, it was found that the supergradient jet was generally located in the left forward quad-

rant of the storm (in the Northern Hemisphere), away from the strongest (earth relative) near-surface winds in the right forward quadrant. The majority of the asymmetric flow was shown to be contained in the deeper of the two asymmetric components, with the shallower one being much weaker. The asymmetric components were interpreted as frictionally stalled inertia waves, where the decay and rotation depth scales adjust so as to provide precisely enough retardation to bring the wave to a halt. The asymmetric components introduce a wave number one asymmetry to the vertical motion, which is superimposed on that due to the symmetric component. The updraft is greatly strengthened in the right forward quadrant, while weak subsidence occurs to the left rear. This may contribute to the observed convective asymmetries in the tropical cyclone eyewall.

Surface wind reduction factors were calculated for stationary and moving storms, and the largest values were found to be near the radius of maximum winds, and on the left, or weaker, side of the storm (Northern Hemisphere). The use of a universal constant for surface wind reduction is thus not supported by the linear model presented here. The variability in the reduction factor between different observational studies is similar to that found here, while the factor most commonly called upon to explain the variations in those studies, namely, the static stability, is not present here. Thus these dynamical factors may be the primary cause of the observed variability.

Acknowledgments. This work was partially supported by the U.S. Office of Naval Research under Grant N-0014-94-1-0493 and forms part of the Australian Tropical Cyclones Coastal Impacts Project. Thanks are due to Mike Montgomery and an anonymous reviewer for their thorough and helpful reviews.

APPENDIX

The Location of the Maximum Updraft in the Symmetric Component

Eliassen and Lystad (1977, henceforth EL) found in their numerical results that the maximum updraft was always located within the radius of maximum winds of their vortex, and that it moved outward as the vortex became stronger, and inward as the drag coefficient increased. Here, the analytical model is used to explain these results, and show that the maximum updraft lies outside the radius of maximum winds for storms stronger than they considered. From (28) and (30),

$$w_{\infty}(r) = \frac{\chi + 2}{2\chi^2 + 3\chi + 2} \frac{1}{r} \frac{\partial}{\partial r} \left(\frac{rCV^2}{f + V/r + \partial V/\partial r} \right) - \frac{2(\chi^2 + 4\chi + 2)}{(2\chi^2 + 3\chi + 2)^2} \frac{\partial \chi}{\partial r} \frac{CV^2}{f + V/r + \partial V/\partial r}. \quad (\text{A1})$$

EL's vortex is given in dimensional form by $V = rRo/f$

($2(1 + (r/r_m)^2)$), where Ro is the Rossby number and r_m the radius of maximum winds. Ignoring for the moment the radial variation of χ , the updraft is proportional to

$$w'_{\infty}(r) = \frac{1}{r} \frac{\partial}{\partial r} \frac{rCV^2}{f + V/r + \partial V/\partial r} = \frac{CRo^2 f}{r} \frac{\partial}{\partial r} \frac{r^3}{Ro + (1 + (r/r_m)^2)^2}. \quad (\text{A2})$$

Clearly, the shape of this curve as a function of r/r_m depends only upon Ro , and varying the other parameters will change only the magnitude. It is plotted for four different values of Ro in Fig. A1, including EL's maximum of $Ro = 20$; the outward displacement of the maximum for more intense vortices is clear.

Figure A2 shows w_{∞} from (A1) for EL's vortex with $Ro = 20$ and various C . As C increases, the maximum updraft moves inwards and broadens, with w_{∞} being constant through much of the eye for $C = 0.02$. Note that the curves here are not exactly the same as in EL, since (i) in Fig A1 they are effectively the limits as $C \rightarrow 0$; (ii) EL considered a slowly decaying vortex after the boundary layer was spun up, while we give results for a steady-state vortex (iii) EL had an upper boundary at height $4.9\delta_0$ and (iv) EL's results were at the level of maximum updraft, while ours are as $z \rightarrow \infty$, and the updraft slopes slightly outwards with height. Indeed, the updraft locations given in Table 2 of EL are always inside of those calculated with the present model, except in the physically uninteresting $C = 0.2$, $Ro < 10$ cases.

To see why increasing drag coefficient displaces the maximum updraft inwards, consider solid body rotation given by $V = rRo/f/2$, so that

$$\chi = rC \sqrt{\frac{f}{2K}} \frac{Ro}{\sqrt{1 + Ro}} \quad (\text{A3})$$

is proportional to r . Then the first term of w_{∞} in (A1) is proportional to r for small r , while the second behaves as r^2 , so w_{∞} is proportional to r at small radii. As $r \rightarrow \infty$, both terms tend to a constant limit. These changes in radial dependence are contained entirely within the expressions involving χ in (A1), and closer examination shows that w_{∞} is close to constant here once χ exceeds 2. If χ is much less than this at the rmw, w_{∞} will be proportional to r throughout the eye and the maximum updraft will lie near the rmw. As χ at the rmw increases, the updraft near the rmw will begin to decrease as the large r limit begins to be felt. Once χ there reaches 2, the large r limit applies and there is a noticeable inward displacement and broadening of the maximum updraft. Even for a very intense vortex with $Ro = 100$, $f = 3.8 \times 10^{-5} \text{ s}^{-1}$, $K = 20 \text{ m}^2 \text{ s}^{-1}$, $C = 0.005$ and $r = 30 \text{ km}$, we have only $\chi = 1.57$. However, EL allowed C up to 0.2, and found that the part of the eye over which w_{∞} was proportional to r became smaller, and that the maximum updraft moved inward, as C increased. In Fig. A2, the values of χ at the rmw are 0, 0.27, 0.82, and

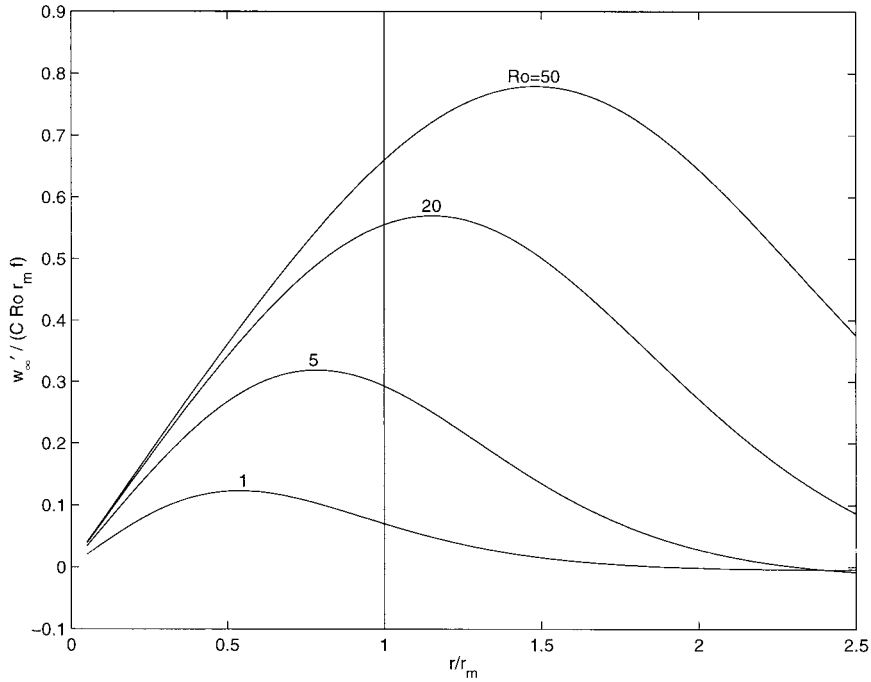


FIG. A1. The approximate updraft in the limit $C \rightarrow 0w'_\infty$, for various Ro as marked (solid), for the vortex of EL. The position of the maximum updraft moves outward with increasing Ro due to the change in relative importance of the planetary and relative vorticities in the denominator of (A2).

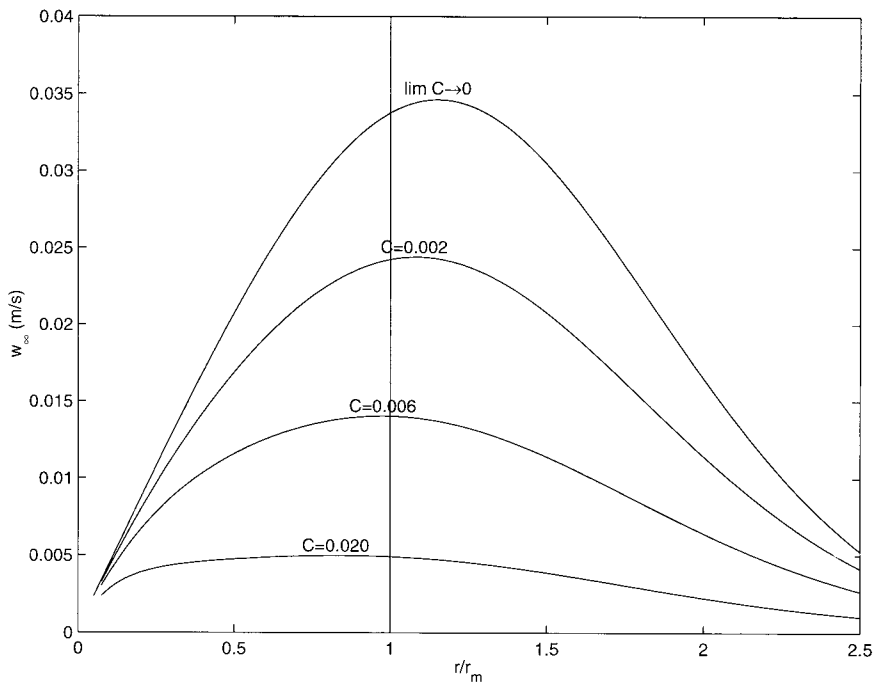


FIG. A2. The updraft w_∞ for the vortex of EL for $Ro = 20$ and $C = 0.002, 0.006, 0.02$, and the approximate updraft w'_∞/C , labeled $C \rightarrow 0$. The parameter χ at the rmw is 0.27, 0.82, and 2.74, respectively, for the curves with nonzero C .

2.72, and only in the last would does w_∞ become approximately constant with radius within part of the eye, consistent with this analysis.

REFERENCES

- Anthes, R. A., and S. Chang, 1978: Response of the hurricane boundary layer to changes of sea surface temperature in a numerical model. *J. Atmos. Sci.*, **35**, 1240–1255.
- Barnes, G. M., and M. D. Powell, 1995: Evolution of the inflow boundary layer of Hurricane Gilbert (1988). *Mon. Wea. Rev.*, **123**, 2348–2368.
- Black, P. G., and G. J. Holland, 1995: The boundary layer of tropical cyclone Kerry (1979). *Mon. Wea. Rev.*, **123**, 2007–2028.
- , and L. K. Shay, 1998: Air–sea interaction processes relevant to tropical cyclone intensity change. Preprints, *Symp. on Tropical Cyclone Intensity Change*, Phoenix, AZ, Amer. Meteor. Soc., 161–168.
- , ———, and V. Pudov, 1993: Observations of air–sea temperature difference in tropical cyclones as a function of wind speed. *Extended Abstracts, Fifth BMRC Modelling Workshop: Parameterisation of Physical Processes*, Melbourne, Australia, Bureau of Meteorology Research Center, 87–88. [Available as Res. Rep. 46 from Bureau of Meteorology Research Center, GPO Box 1289K, Melbourne, Victoria 3001, Australia.]
- Blackadar, A. K., 1957: Boundary layer wind maxima and their significance for the growth of nocturnal inversions. *Bull. Amer. Meteor. Soc.*, **38**, 283–290.
- Brown, R. A., 1970: A secondary flow model for the planetary boundary layer. *J. Atmos. Sci.*, **27**, 742–757.
- , 1972a: On inflection point instability of a stratified Ekman boundary layer. *J. Atmos. Sci.*, **29**, 850–859.
- , 1972b: On the physical mechanism of inflection point instability. *J. Atmos. Sci.*, **29**, 984–986.
- Carrier, G. F., 1971: Swirling flow boundary layers. *J. Fluid. Mech.*, **49**, 133–144.
- Cione, J. J., P. G. Black, and S. H. Houston, 2000: Surface observations in the hurricane environment. *Mon. Wea. Rev.*, **128**, 1550–1561.
- Eliassen, A., 1971: On the Ekman layer in a circular vortex. *J. Meteor. Soc. Japan*, **49**, 784–789.
- , and M. Lystad, 1977: The Ekman layer of a circular vortex: A numerical and theoretical study. *Geophys. Norv.*, **31**, 1–16.
- Faller, A. J., and R. E. Kaylor, 1966: A numerical study of the instability of the laminar Ekman boundary layer. *J. Atmos. Sci.*, **23**, 466–480.
- Frank, W. M., 1984: A composite analysis of the core of a mature hurricane. *Mon. Wea. Rev.*, **112**, 2401–2420.
- Garratt, J. R., 1977: Review of drag coefficients over oceans and continents. *Mon. Wea. Rev.*, **105**, 915–929.
- Gray, W. M., 1967: The mutual variation of wind, shear, and baroclinicity in the cumulus convective atmosphere of the hurricane. *Mon. Wea. Rev.*, **95**, 55–73.
- , 1991: Comments on “Gradient balance in tropical cyclones.” *J. Atmos. Sci.*, **48**, 1201–1208.
- , and D. S. Shea, 1973: The hurricane’s inner core region. Part II: Thermal stability and dynamic characteristics. *J. Atmos. Sci.*, **30**, 1565–1576.
- Harper, B. A., K. F. Lovell, B. D. Chandler, and D. J. Todd, 1989: The derivation of environmental design criteria for Goodwyn A platform. *Proc. 9th Australian Conf. on Coastal and Ocean Engineering*, Adelaide, Australia, The Institution of Engineers, Australia, 364–368. [Available from The Institution of Engineers, Australia, 11 National Circuit, Barton, ACT 2600, Australia.]
- , L. B. Mason, and L. Bode, 1993: Tropical Cyclone Orson—A severe test for modelling. *Proc. 11th Australian Conf. on Coastal and Ocean Engineering*, Townsville, Australia, The Institution of Engineers, Australia, 59–64. [Available from The Institution of Engineers, Australia, 11 National Circuit, Barton, ACT 2600, Australia.]
- Hawkins, H. F., and D. T. Rubsam, 1968: Hurricane Hilda, 1964. II. Structure and budgets of the hurricane on October 1, 1964. *Mon. Wea. Rev.*, **96**, 617–636.
- Hock, T. F., and J. L. Franklin, 1999: The NCAR GPS dropwindsonde. *Bull. Amer. Meteor. Soc.*, **80**, 407–420.
- Holland, G. J., 1980: An analytic model of the wind and pressure profiles in hurricanes. *Mon. Wea. Rev.*, **108**, 1212–1218.
- Hubbert, G. D., G. J. Holland, L. M. Leslie, and M. J. Manton, 1991: A real-time system for forecasting tropical cyclone storm surges. *Wea. Forecasting*, **6**, 86–97.
- KePERT, J. D., and Y. Wang, 2001: The dynamics of boundary layer jets within the tropical cyclone core. Part II: Nonlinear enhancement. *J. Atmos. Sci.*, **58**, 2485–2501.
- Korolev, V. S., S. A. Petrichenko, and V. D. Pudov, 1990: Heat and moisture exchange between the ocean and atmosphere in tropical storms Tess and Skip. *Meteor. Gidrol.*, **2**, 108–111. (English translation in *Sov. Meteor. Hydrol.*, **2**, 92–94).
- Large, W. G., and S. Pond, 1981: Open ocean momentum flux measurements in moderate to strong winds. *J. Phys. Oceanogr.*, **11**, 324–336.
- La Seur, N. E., and H. F. Hawkins, 1963: An analysis of Hurricane Cleo (1958) based on data from research reconnaissance aircraft. *Mon. Wea. Rev.*, **91**, 694–709.
- Li, J., N. E. Davidson, G. D. Hess, and G. Mills, 1997: A high-resolution prediction study of two typhoons at landfall. *Mon. Wea. Rev.*, **125**, 2856–2878.
- Lilly, D. K., 1966: On the instability of Ekman boundary layer flow. *J. Atmos. Sci.*, **23**, 481–494.
- Marks, F. D., P. Dodge, and C. Sandin, 1999: WSR-88D observations of hurricane atmospheric boundary layer structure at landfall. Preprints, *23d Conf. on Hurricanes and Tropical Meteorology*, Dallas, TX, Amer. Meteor. Soc., 1051–1054.
- Mitsuta, Y., T. Suenobu, and T. Fujii, 1988: Supergradient surface wind in the eye of a typhoon. *J. Meteor. Soc. Japan*, **66**, 505–508.
- Moss, M. S., and F. J. Merceret, 1976: A note on several low-level features of Hurricane Eloise (1975). *Mon. Wea. Rev.*, **104**, 967–971.
- Powell, M. D., 1980: Evaluations of diagnostic marine boundary-layer models applied to hurricanes. *Mon. Wea. Rev.*, **108**, 757–766.
- , 1982: The transition of the Hurricane Frederic boundary-layer wind fields from the open Gulf of Mexico to landfall. *Mon. Wea. Rev.*, **110**, 1912–1932.
- , 1987: Changes in the low-level kinematic and thermodynamic structure of Hurricane Alicia (1983) at landfall. *Mon. Wea. Rev.*, **115**, 75–99.
- , 1990a: Boundary layer structure and dynamics in outer hurricane rainbands. Part I: Mesoscale rainfall and kinematic structure. *Mon. Wea. Rev.*, **118**, 891–917.
- , 1990b: Boundary layer structure and dynamics in outer hurricane rainbands. Part I: Downdraft modification and mixed layer recovery. *Mon. Wea. Rev.*, **118**, 918–938.
- , P. D. Dodge, and M. L. Black, 1991: The landfall of Hurricane Hugo in the Carolinas: Surface wind distribution. *Wea. Forecasting*, **6**, 379–399.
- , S. H. Houston, and T. A. Reinhold, 1996: Hurricane Andrew’s landfall in south Florida. Part I: Standardizing measurements for documentation of surface wind fields. *Wea. Forecasting*, **11**, 304–328.
- Rosenthal, S. L., 1962: A theoretical analysis of the field of motion in the hurricane boundary layer. National Hurricane Research Project Rep. 56, U.S. Dept. of Commerce, 12 pp.
- Shapiro, L. J., 1983: The asymmetric boundary layer under a translating hurricane. *J. Atmos. Sci.*, **40**, 1984–1998.
- Shea, D. J., and W. M. Gray, 1973: The hurricane’s inner core region.

- I. Symmetric and asymmetric structure. *J. Atmos. Sci.*, **30**, 1544–1564.
- Smith, R. K., 1968: The surface boundary layer of a hurricane. *Tellus*, **20**, 473–483.
- Snell, H. D., and M. T. Montgomery, 1999: Spin-down dynamics of axisymmetric hurricanes. Preprints, *23d Conf. on Hurricanes and Tropical Meteorology*, Dallas, TX, Amer. Meteor. Soc., 1031.
- Taylor, G. I., 1914: Eddy motion in the atmosphere. *Philos. Trans. Roy. Soc.*, **240A**, 1–26.
- Willoughby, H. E., 1990: Gradient balance in tropical cyclones. *J. Atmos. Sci.*, **47**, 265–274.
- , 1991: Reply. *J. Atmos. Sci.*, **48**, 1209–1212.
- Wilson, K. J., 1979: Characteristics of the subcloud layer wind structure in tropical cyclones. *Extended Abstracts, Int. Conf. on Tropical Cyclones*, Perth, Australia, Roy. Meteor. Soc. (Australian Branch), 15II.
- Wurman, J., and J. Winslow, 1998: Intense sub-kilometre-scale boundary layer rolls observed in Hurricane Fran. *Science*, **280**, 555–557.